# Observation of enhanced ferromagnetic spin-spin correlations at a triple point in quasi-two-dimensional magnets

Yugang Zhang,[1,2] Zefang Li,[3] Jing Zhang,[1,2] Ning Cao,[2] Long Zhang,[1,2] Yonghong Li,[1,2] Shuang Liu,[2] Xiaoyuan Zhou,[2] Young Sun [2,*], Wenhong Wang,[3,4,†] and Yisheng Chai [1,2,‡]

[1]*Low Temperature Physics Laboratory, College of Physics, Chongqing University, Chongqing 401331, China*
[2]*Center of Quantum Materials and Devices, Chongqing University, Chongqing 401331, China*
[3]*Beijing National Laboratory for Condensed Matter Physics, Institute of Physics, Chinese Academy of Sciences, Beijing 100190, China*
[4]*School of Electronics & Information Engineering, Tiangong University, Tianjin 300387, China*

The magnetic field-temperature phase diagrams and spin-spin correlations of quasi-two-dimensional ferromagnetic $Cr_2Ge_2Te_6$ and $Cr_2Si_2Te_6$ and antiferromagnetic $MnBi_2Te_4$ are investigated and compared by a sensitive composite magnetoelectric method. The phase diagrams of $Cr_2Ge_2Te_6$ and $Cr_2Si_2Te_6$ disclose a triple point around the Curie temperature where three phases coexist, for both $H \parallel c$ axis and $ab$ plane configurations. In contrast, a triple/tricritical point is found in $MnBi_2Te_4$ only for the $H \parallel c$ axis configuration. Anomalous enhancement of magnetoelectric signals is observed near the triple points of $Cr_2Ge_2Te_6$ and $Cr_2Si_2Te_6$, suggesting significant enhancement of ferromagnetic spin-spin correlations at this point. Nevertheless, no short-range spin-spin correlation is found in $MnBi_2Te_4$ above the Néel temperature.

## I. INTRODUCTION

Recently, the easy-exfoliated layered two-dimensional (2D) magnetic materials such as $CrI_3$ [1], $Cr_2Ge_2Te_6$ (CGT) [2], $Cr_2Si_2Te_6$ (CST) [3], $Fe_3GeTe_2$ [4], and $MnBi_2Te_4$ (MBT) [5], etc., have attracted considerable research interest. Even though the Ginzburg criterion states that 2D spin systems are much more vulnerable to fluctuations in magnetic order parameters [6], low dimensional long-range magnetic order in a few atomic layers has already been observed experimentally due to the strong magnetic anisotropy [2]. Zero field quantum anomalous Hall effect is also observed in the antiferromagnetic topological insulator $MnBi_2Te_4$ [5]. These materials provide ideal platforms for exploring the strong magnetic fluctuations down to the 2D limit [2,7] and show great promise for future spintronic and topological applications.

$MnBi_2Te_4$ is a van der Waals layered antiferromagnetic (AFM) topological insulator which belongs to the space group $R\text{-}3m$, as shown in Fig. 1(a). Its Mn spins order antiferromagnetically along the $c$ axis at $T_N = 25$ K [8]. Chromium tellurides $Cr_2Ge_2Te_6$ and $Cr_2Si_2Te_6$ are uniaxial ferromagnetic (FM) semiconductors [9] and belong to the class of layered transition metal trichalcogenides, which are crystallized in the trigonal space group $R\text{-}3$, as shown in Fig. 1(b). $Cr^{3+}$ is responsible for the spontaneous magnetic order under zero magnetic field ($H$) at $T_C = 34$ K and 67 K for CST and CGT, respectively, with the easy axis aligning along the

$c$ axis [10]. The short-range spin-spin correlations and critical components of CST and CGT at $T_C$ under an out-of-plane magnetic field ($H \parallel c$) have been comprehensively investigated [11–14]. In contrast, the equivalent correlation and critical behaviors of MBT have rarely been studied due to its AFM nature. Moreover, such differences between FM and AFM orderings have yet to be compared.

Fluctuations and correlations, usually strongly relying on the dimension, may exhibit different behavior in FM and AFM systems. In previous studies, the spin-spin correlations above $T_C$ in CGT and CST were revealed in static magnetic susceptibility [10], $X$-band electron spin resonance [9], second harmonic generation [15], thermal expansion [16], etc. However, magnetic fluctuations in MBT are only significant in reduced thickness down to two-septuple layers found in Raman spectroscopy measurements [17]. According to Callen's model, the correlation function of spins around magnetic transition temperature can be reflected in magnetoelastic properties due to spin-lattice coupling from exchange interactions [18]. By measuring the thermal expansion $\lambda = dL/L$ ($L$ is the sample length) with capacitance dilatometry in CGT, the nonzero $d\lambda/dT$ far above $T_C$ due to short-range spin-spin correlations was confirmed [16]. Therefore, more elastic properties are expected to be affected by spin-spin correlations in these systems.

In principle, the piezomagnetic coefficient ($=d\lambda/dH$) is also closely related to magnetic interactions and often discussed in terms of strain dependence of free energy. Differences in the spin-spin correlations between FM and AFM systems are expected [19]. Therefore, investigating magnetostrictive properties of different magnetic orderings may unveil the physics behind their fluctuation behaviors, particularly around magnetic phase transitions. However, the direct

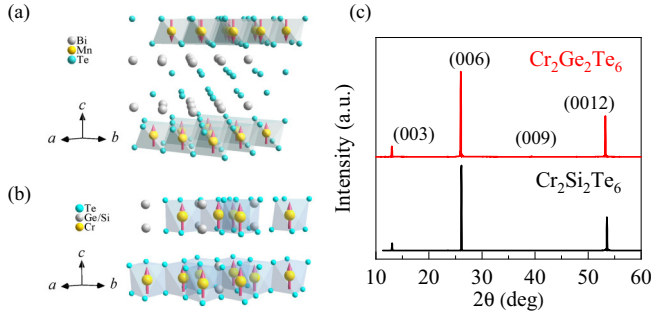*youngsun@cqu.edu.cn
†wenhongwang@tiangong.edu.cn
‡yschai@cqu.edu.cn

FIG. 1. Crystal structures of (a) $MnBi_2Te_4$, (b) $Cr_2Si_2Te_6$ and $Cr_2Ge_2Te_6$. (c) Single crystal x-ray diffractions of $Cr_2Ge_2Te_6$ and $Cr_2Si_2Te_6$.

measurement of magnetostriction by capacitance dilatometry is challenging for thin flake 2D materials.

Recently, an ac technique of piezoelectric transducer [20], based on the traditional magnetoelectric (ME) composite configuration [21], has been developed to sense the ac in-plane piezomagnetic coefficient $d\lambda/dH$ of magnetic materials via interfacial strain coupling. This technique has been applied to obtain magnetic phase diagrams of bulk MnSi samples and successfully identified their skyrmion phases and regions with short-range spin-spin correlations [20]. In this paper, we demonstrate remarkable differences in the phase diagram, critical behavior, and spin-spin correlations of FM $Cr_2Ge_2Te_6$ and $Cr_2Si_2Te_6$ and AFM $MnBi_2Te_4$ single crystals by this ME composite technique. Three phase boundaries, characterized by clear peaks/steps in the real part of ac ME signals, meet at a triple point around $T_C$ or $T_N$. The ME signals become maximum at the triple points in $Cr_2Ge_2Te_6$ and $Cr_2Si_2Te_6$, implying a significant enhancement of ferromagnetic spin-spin correlations at this point. In contrast, no spin fluctuation in $MnBi_2Te_4$ is found at the triple point or above $T_N$. Moreover, a crossover line between ferromagnetic and paramagnetic (PM) phases is omitted in $MnBi_2Te_4$.

## II. METHODS

Single crystals of MBT, CST, and CGT were grown by the self-flux method [8,22], and the quality of CST and CGT crystals were checked by x-ray diffraction, as shown in Fig. 1(c). The quality of MBT single crystal was checked in the literature [8]. Magnetostriction is detected by a dilatometer using a capacitance bridge (AH2550A, Andeen-Hagerling, Inc.). The temperature and magnetic field environments are supplied by a 9 T Dynacool system (Quantum Design). In the composite magnetoelectric method, CST, CGT, and MBT, as the magnetostrictive phases, are glued onto a 0.2-mm-thick piezoelectric layer of $0.7Pb(Mg_{1/3}Nb_{2/3})O_3 - 0.3PbTiO_3$ (PMN-PT) [001]-cut single crystal [see the inset of Fig. 2(b)]. Ag epoxy (H20E, Epoxy Technology Inc.) acts as the electrode and a strain mediator. Before electrical measurements, the PMN-PT was electrically poled under an electric field of 550 kV/m. The electrical signal of ME laminates $V_{ME} = V_x + iV_y$ ($V_x$ and $V_y$ represent in-phase and out-of-phase signals, respectively) are measured by a lock-in amplifier (OE1022, SYSU Scientific Instruments) with a
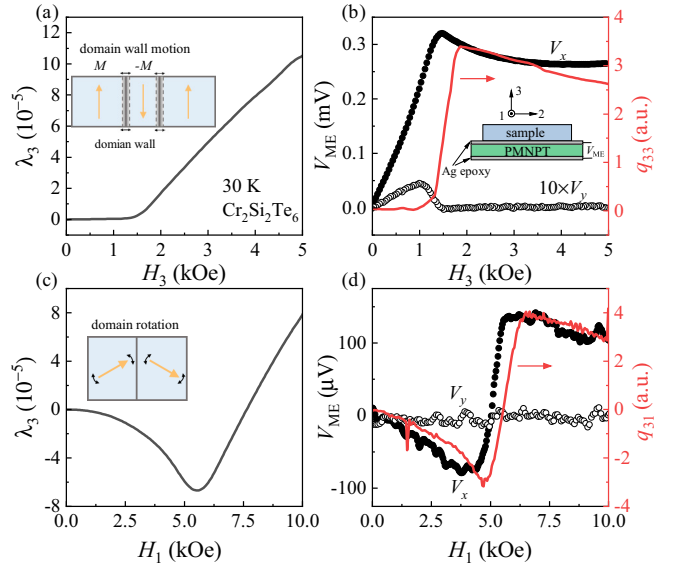
commercial sample stick (MultiField Tech.). An ac magnetic field $H_{ac} = 1$ Oe is generated by a Helmholtz coil.

## III. RESULTS AND DISCUSSION

### A. Magnetization measurements of CGT and CST

Temperature-dependent magnetization after field cooling of CGT and CST, for the magnetic field along the $ab$ plane ($H_1$) and $c$ axis ($H_3$) with $H = 0.1$ kOe, is presented in Figs. 3(a) and 3(b), respectively. A typical PM to FM phase transition occurs at $T_C = 34$ K and 67 K for CST and CGT, respectively, consistent with previous reports [13,23]. In the



FIG. 2. (a),(c) $H$ dependent magnetostriction $\lambda_3$ for $H\|c$ axis and $H\|ab$ plane of $Cr_2Si_2Te_6$ at 30 K, respectively. (b), (d) $V_{ME}$ signals for the $H_3$ and $H_1$ configurations at 30 K, respectively. The piezomagnetic coefficients $q_{ij}$ are also plotted for comparison.
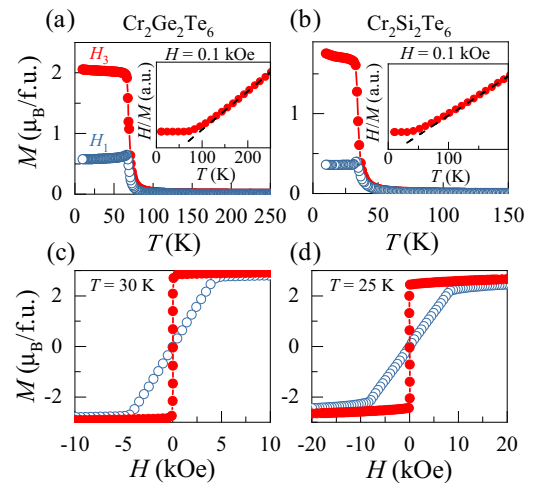


FIG. 3. $T$-dependent magnetization of (a) $Cr_2Ge_2Te_6$ and (b) $Cr_2Si_2Te_6$ measured at $H = 0.1$ kOe for both $H\|ab$ plane and $H\|c$ axis. $H$-dependent magnetization of (c) $Cr_2Ge_2Te_6$ and (d) $Cr_2Si_2Te_6$ measured at $T = 30$ and 25 K, respectively.

$H_3$ configuration, the $H/M$ curves in both compounds [insets of Figs. 3(a) and 3(b)] deviate from the linear fit below 150 K, confirming a short-range spin-spin correlation in the PM phase far above $T_C$ [10,11]. Moreover, the isothermal magnetization curves are measured for CGT and CST at 30 and 25 K, respectively [Figs. 3(c) and 3(d)]. The saturation fields of both compounds in the $H_3$ configuration (2.0 and 2.5 kOe, respectively) are much smaller than those in the $H_1$ configuration (8.0 and 4.5 kOe, respectively), showing the $c$-axis magnetic anisotropy and different magnetization processes [13,23]. The drastic difference in the saturation fields indicates different microscopic domain dynamics in the magnetization process. The corresponding magnetization data for the antiferromagnetic MBT has already been reported in Ref. [8]. The spin-spin correlations and domain-related dynamics can be generally reflected in the magnetoelastic channel. Therefore, magnetostrictive measurements may provide insight information on those magnetically ordered systems.

### B. Magnetoelectric and magnetostrictive measurements in field scan

In principle, due to the geometry of the laminate configuration, only the in-plane magnetostrictive behaviors can be transferred to the piezoelectric layers via interfacial strain coupling and involve in the ME signals while the out-of-plane magnetostriction cannot. When the ac-driven magnetic field is applied to the laminate, the resultant $V_{ME}$ is directly proportional to the sample's piezomagnetic coefficient $d\lambda/dH$. In the $H_1$ and $H_3$ configurations [24]

$$V_{ME33} \propto kd_{31}q_{13} \text{ and } V_{ME31} \propto -kd_{31}(q_{11} + q_{21}), \quad (1)$$

where $k$ is the interface strain coupling parameter ($0 < k < 1$ and $k = 1$ for ideal coupling), $V_{MEij}$ is the voltage measured along the $i$ axis for $H$ applied along the $j$ axis, $d_{31}$ is the transverse piezoelectric coefficient, $q_{ij}$ are the piezomagnetic coefficients, i.e., $d\lambda_i/dH_j$, where $\lambda_i$ is the magnetostriction along the $i$ axis for $H$ along the $j$ axis. Therefore, $V_{ME33}(H)$ and $V_{ME31}(H)$ can effectively reflect piezomagnetic coefficients $q_{13}(H)$ and $[q_{11}(H) + q_{21}(H)]$, respectively. Besides the piezomagnetic coefficients, according to these equations, the measured voltage values depend largely on the sample preparation processes. (i) The quality of the interfacial contact condition, which is reflected in $k$, can be improved by increasing the roughness of the interface and the stiffness of the epoxy. (ii) The piezoelectric coefficient: Large transverse piezoelectric coefficients can be obtained by poling the piezoelectric layer with a large electric field at room temperature. However, each time, the resultant coefficients cannot be the same for the same piece, not to mention the variation between different pieces. Therefore, the reproducibility of the data is very unlikely when the composite is reassembled and has to be poled once again. It is highly recommended to perform all the measurements in one time at the low-temperature region because the interfacial coupling and piezoelectric coefficients are stable enough below 100 K without warming to room temperature. The measured signals can be well reproduced upon successive thermal and magnetic field cycles at this temperature region. It is still physically meaningful to compare

the ME signals at each temperature and magnetic field within one measurement.

To exemplify the relationship between in-plane $q_{ij}$ and $V_{ME}$ in a magnetically ordered system, the $H$ dependent $\lambda_3$ of CST for $H_3$ and $H_1$ at 30 K are measured [Figs. 2(a) and 2(c), respectively]. $\lambda_3$ of CST in both configurations shows a clear kink around the saturation field, connecting a linear behavior with a positive slope for the higher field. The corresponding $q_{33}$ and $q_{31}$ are calculated [Figs. 2(b) and 2(d), respectively]. Then, we mechanically bond the CST sample with a piece of PMN-PT to form a composite ME configuration. $V_{ME}$ under the same conditions are measured to compare with $q_{33}$ and $q_{31}$ curves [Figs. 2(b) and 2(d), respectively]. In the $H_3$ case, $V_x$ shows distinct peak behavior with that of $q_{33}$ in the low field region, indicating that the out-of-plane magnetostriction has nothing to do with the ME signal. In the $H_1$ case, $V_x$ shows an almost identical sign-reversal profile to that of $q_{31}$, as shown in Fig. 2(d). We note that $\lambda_1(H) + \lambda_2(H) + \lambda_3(H) \approx 0$ due to the volume conservation of the sample under the application of the in-plane $H_1$. Then, Eq. (1) can be transformed to $V_{ME31} \propto q_{31}$, which is consistent with our experimental results. In brief, the composite ME method is a highly sensitive ac technique for probing in-plane magnetostrictive properties.

Further analysis of the ME data can reveal more underlying information in CST. In the $H_3$ case, inconsistency between $V_x$ and $q_{33}$ points to a uniaxial ferromagnetic nature of CST that the domain wall motion process [inset of Fig. 2(a)] under $H_3$ leads to a negligible $\lambda_3$ and a field dependent $\lambda_1$. Furthermore, it is well known that the domain wall movement in small $H_3$ (<1.5 kOe) will dissipate energy from depinning behaviors, resulting in a nonzero $V_y$ in the multidomain state in Fig. 2(b). In the $H_1$ case, Selter *et al.* [10] suggest that the domain rotation process is dominating before saturation (<5.5 kOe), as shown in the inset of Figs. 2(c) and 3. This is supported by the zero-$V_y$ value in the whole field regions. Besides, after saturating in the spin-polarized (SP) state, $V_x$ is nonzero up to the highest field. The magnetostriction in the SP phase should be dominated by forced volume magnetostriction governed by exchange energy [25]. In other words, the ME signals of the composite are sensitive not only to the domain dynamics but also to the microscopic spin-spin interactions. It is suitable to study the possible spin fluctuations in AFM and FM systems in quasi-2D nature.

The $V_{ME}$ as a function of $H_1$ and $H_3$ for CST at other temperatures are shown in Fig. 4(a). Below $T_C$, $V_x$ of CST in the $H_3$ configuration always shows a peak feature that increases in magnitude and moves to lower fields with increasing temperature. In the $H_1$ configuration, there are two peaks in $V_x$; the negative one is weakened while the positive one is enhanced, and both of them move to lower fields with increasing temperature. All the features are consistent with Figs. 2(b) and 2(d), and the positive peak fields coincide well with the saturation fields obtained from the $M$-$H$ curves, as shown in Fig. 3(c). Interestingly, above $T_C$ in the PM phase where no long-range magnetic ordering exists, all the $V_x$ signals still show considerable intensity with broad bump features moving to higher fields with increasing temperature. The ME signals above $T_C$ indicate a strong short-range spin-spin correlation in this FM system [15]. We also measured CGT with similar
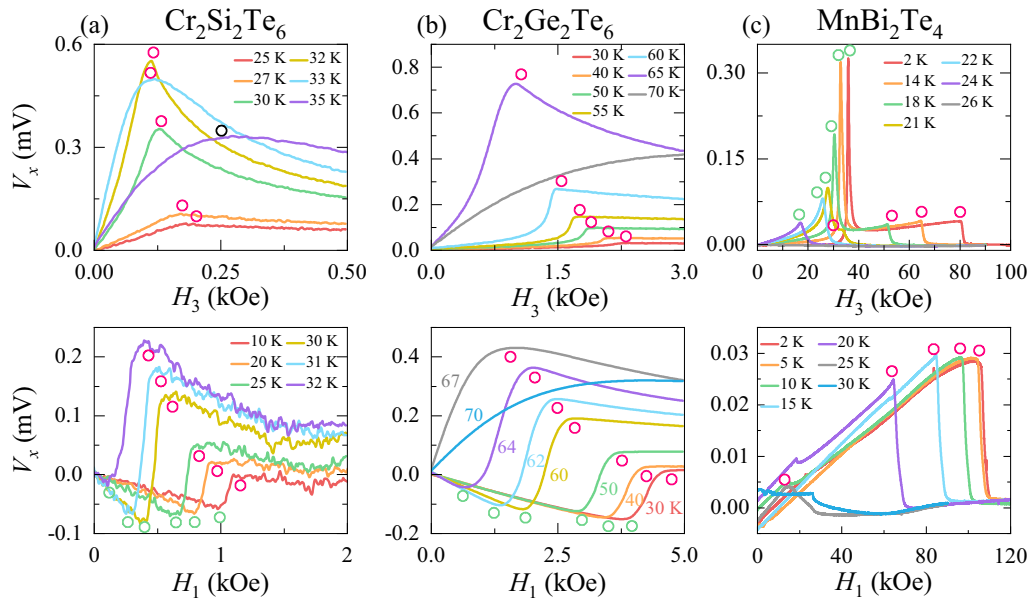
FIG. 4. $H$-dependent $V_x$ of (a) $Cr_2Si_2Te_6$, (b) $Cr_2Ge_2Te_6$, and (c) $MnBi_2Te_4$ measured at selected $T$. The upper panels are the real part $V_x$ in the $H_3$ configuration. The lower panels are $V_x$ in the $H_1$ configuration. The open circles represent transition or saturation fields.

FM ordering, which exhibits all the similar features below and above $T_C$, as shown in Fig. 4(b).

In comparison, the $V_{ME}$ as a function of $H_1$ and $H_3$ for antiferromagnetic $MnBi_2Te_4$ are measured in both configurations [Fig. 4(c)]. At low temperatures, there are a sharp peak and a step in $V_x$ with $H_3$ configuration, marking a spin flop transition into a canted antiferromagnetic (c-AFM) phase and the saturation of magnetization, respectively. The transition fields are consistent with previous $M$-$H$ measurements in the literature [8]. Both features move to lower $H$ with increasing $T$, merge at around 23 K, and disappear above $T_N$. In the $H_1$ configuration, the only step in $V_x$ indicates the saturation of $M$. It moves to the lower field in higher $T$ and disappears above $T_N$. Contrarily to the case of CGT and CST, $V_x$ of MBT immediately becomes negligibly small in both the spin fully polarized FM state below $T_N$ and PM state above $T_N$. Such discrepancy in $V_x$ between FM and AFM systems should come from the lack of short-range spin-spin correlations above $T_N$ and the lack of forced volume magnetostriction after the saturating of $M$ in $MnBi_2Te_4$.

### C. Magnetoelectric measurements in temperature scan

To further reveal the discrepancy between the two systems around magnetic ordering temperatures, the $V_{ME}$ as a function of temperature under various fields for $H_1$ and $H_3$ are shown in Fig. 5. For CST, all $V_x$ show a pronounced broad peak around $T_C$ which shifts to lower temperatures in small magnetic fields ($H_3 < 2$ kOe and $H_1 < 1$ kOe) and moves towards higher $T$ in stronger $H$ [Fig. 5(a)]. This peak feature is consistent with the broad bump in the $H$ scan above $T_C$. The nonzero $V_x$ can persist up to two times $T_C$, implying the strong spin-spin correlations up to those temperatures. The CGT data show a similar trend in Fig. 5(b). For MBT with cooling in Fig. 5(c), $V_x$ is zero above $T_N$, gets a sudden enhancement at $T_N$, and then slowly decays in the ordered phases in both configurations. These

steplike features in $V_x$ shift to lower $T$ with increasing $H$. The immediate vanishing of $V_x$ in the PM phase confirms a complete suppression of spin-spin correlation in this system. Besides, in 30 K with $H_3$ configuration, a second more substantial peak is found below $T_N$, representing the spin-flop transition in the $H$ scan data. All other features are entirely consistent between the $H$ scan and $T$ scan data in the three systems.

### D. Phase diagram and contour plot

Accordingly, the $H$-$T$ phase diagrams of CGT, CST, and MBT are constructed from the above measurements, as shown in Fig. 6. In CGT and CST, paramagnetic, SP single domain, and ferromagnetic phases with domains and domain walls (DWs) are identified. The three phases' boundaries are determined from the peak position of $V_x$ peaks and are in good agreement with magnetization and ferromagnetic resonance (FMR) measurements [19]. In each phase of FM compounds, $V_{ME}$ has different microscopic origins. For CGT and CST, as exemplified in Fig. 2, the $V_{ME}$ of FM phases in $H_3$ and $H_1$ configurations are dominated by DW motion and domain rotation, respectively. The $V_x$ signal is smaller under lower $T$ due to the freezing of thermal energy. In the spin-polarized state, $V_x$ is governed by volume magnetostriction behaviors and is weaker under higher $H$ due to the competition between thermal energy and Zeeman energy. In the PM phase, $V_x$ is weaker in higher $T$ and may be due to the suppression of short-range spin-spin correlations by thermal fluctuation.

In the $H_3$ configuration [Figs. 6(a) and 6(b)], all three lines converge at one point, which is very likely to be a triple point (TP). In the $H_1$ configuration [Figs. 6(d) and 6(e)], there is an extra line within the FM phase. This line was attributed to a phase boundary between FM and other phases in the literature [10]. However, our FMR and magnetization data in the $H$ scan support a boundary defined by the positive peak in $V_x$ with
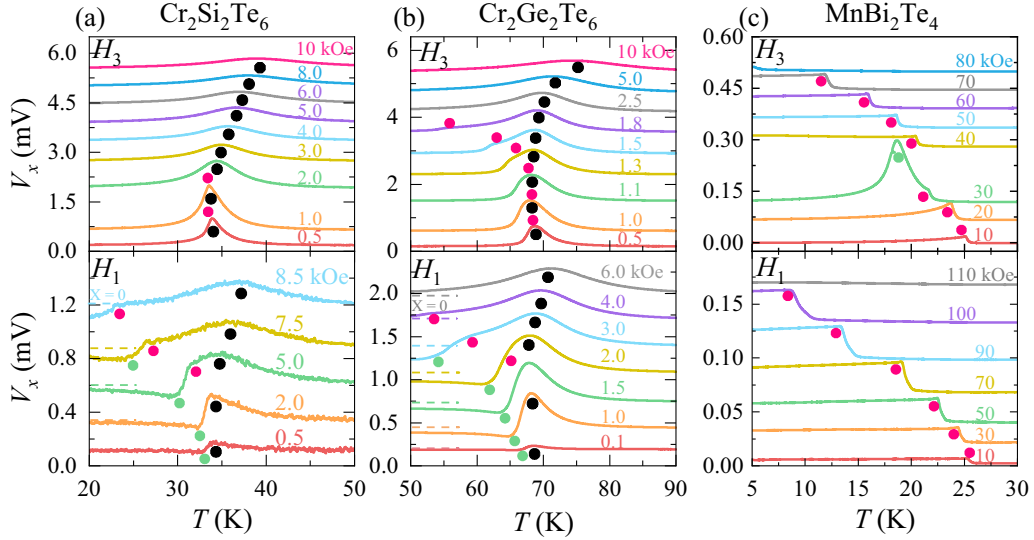
FIG. 5. $T$-dependent $V_x$ signals of (a) $Cr_2Si_2Te_6$, (b) $Cr_2Ge_2Te_6$, and (c) $MnBi_2Te_4$ measured at selected $H$. The upper panels are $V_x$ in the $H_3$ configuration. The lower panels are $V_x$ in the $H_1$ configuration. All plots have been shifted vertically for clarity. The solid circles represent transition or saturation temperatures.

larger field values [19]. As a result, a TP also exists in the $H_1$ configuration for CGT and CST, where three boundaries meet at one point. In MBT, on the other hand, PM, AFM, c-AFM, and FM phases are identified. In the $H_3$ configuration, a spin-flop transition line separates the AFM and c-AFM phases. This line meets with two other phase boundaries to form a TP point near $T_N$. The nature of this line should be in the first order. However, no hysteresis behavior is found in the ME signals at 2 K, as depicted in Fig. 7(a). That may be due to the nucleation process of the domains [26], and we

indeed find a significant $V_y$ near this transition due to domain wall motion. With increasing $T$, the spin flop transition (AFM to c-AFM phase transition) gradually smears out, making it a second order around its end point. Therefore, this TP point is very likely tricritical as well. The $H_1$ configuration has no TP or tricritical point with a trivial phase diagram. The most significant difference between the phase diagrams of FM and AFM ordering is the lack of a crossover line between FM and PM phases in the AFM system. Thus, the related TP points are also missing in MBT.
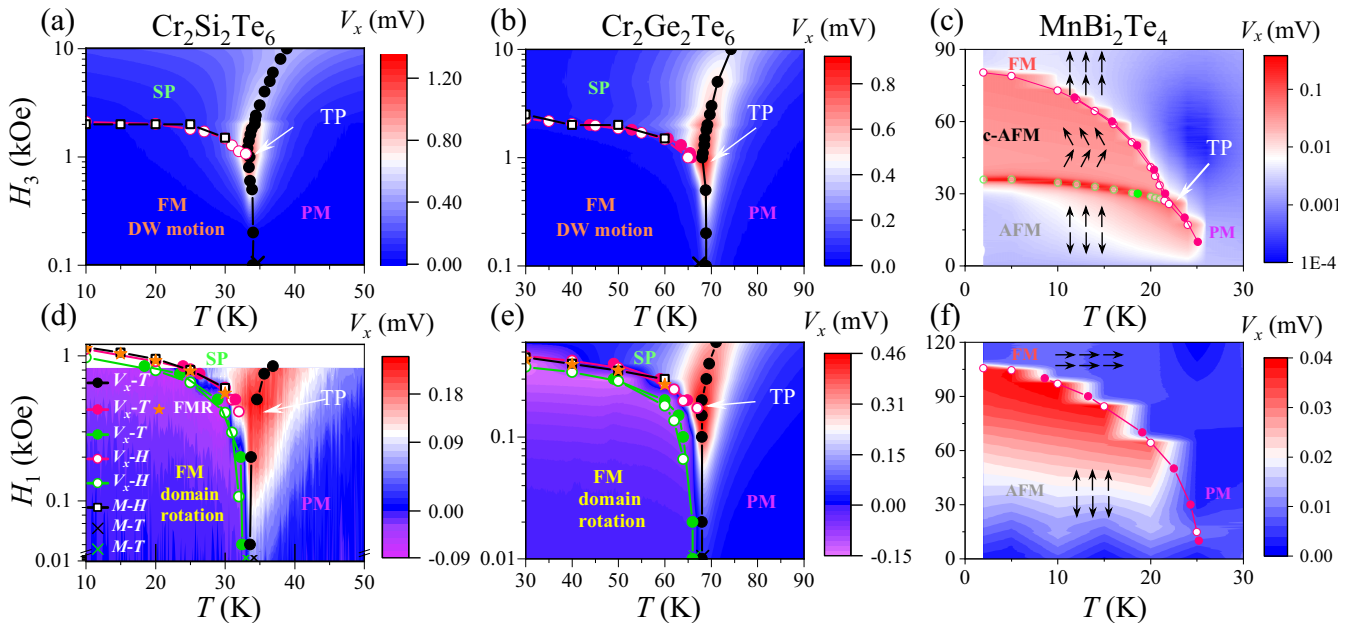


FIG. 6. Phase diagrams of $Cr_2Si_2Te_6$ for (a) $H\|c$ axis and (d) $H\|ab$ plane, that of $Cr_2Ge_2Te_6$ for (b) $H\|c$ axis and (e) $H\|ab$ plane, and that of $MnBi_2Te_4$ for (c) $H\|c$ axis and (f) $H\|ab$ plane. The background of the phase diagrams of $Cr_2Ge_2Te_6$ and $Cr_2Si_2Te_6$ are the contour plots of $V_x-T$ data, while the background of the phase diagrams of $MnBi_2Te_4$ are the contour plots of $V_x-H$ data.
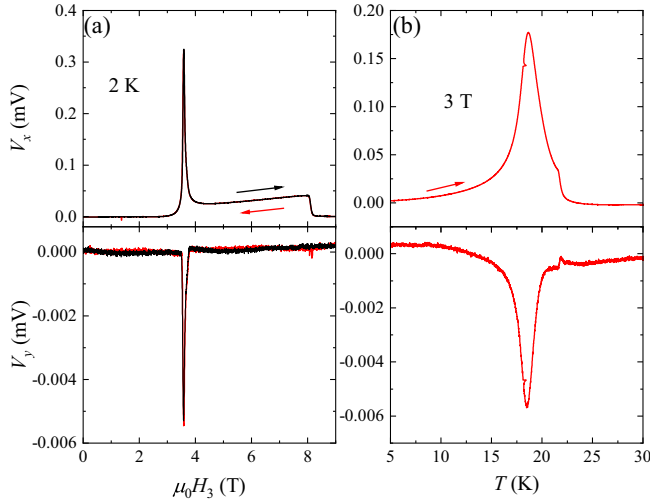
FIG. 7. $H$ scan (a) and $T$ scan (b) data of $V_x$ and $V_y$ of MnBi$_2$Te$_4$ measured under the $H_3$ configuration.

To reveal the influence of two kinds of TPs on the magnetostrictive properties, we draw the contour plot of $V_x - T$ as the background in the phase diagrams of CGT and CST, and $V_x - H$ as the background in the phase diagrams of MBT, as shown in Fig. 6. For CGT and CST, all the tendencies point to enhanced $V_x$ signals around the TPs, which can be understood from their phase coexistence nature. That is very similar to the morphotropic phase boundary in ferroelectrics [27], where the coexistence of competing phases is very susceptible to an external stimulus, so enhanced piezoelectricity is induced. As a result, the largest $V_x \propto d\lambda/dH$ appears at TPs in CST and CGT. In contrast, in the AFM MBT, there is no significant intensity in the entire FM/PM region, which makes the disappearance of any crossover line between FM and PM phases. That clearly rules out any short-range correlation above $T_N$. Moreover, from the ordered side of the phase diagram, there is no enhancement of $V_x$ near the TP of MBT in the $H_3$ configuration either. That is quite counterintuitive in that the TP of MBT closes to/is a tricritical point with critical fluctuations. It seems that the fluctuation, if there is any in MBT, cannot be revealed in magnetostrictive properties. By referring to a similar Ising AFM UIrSi$_3$ system, its elastic moduli instead of $d\lambda/dH$ are significantly enhanced at a similar tricritical point due to the spin-flip transition [28]. Therefore, the pure elastic channel may be more suitable for investigating of critical fluctuation in an AFM system.

### E. Discussion

From the perspective of thermodynamics, the expression of the piezomagnetic coefficient $\frac{\partial \lambda}{\partial H}$ near $T_C$ is derived by [29]

$$\frac{\partial \lambda}{\partial H} \approx \frac{\rho M_s}{\rho_0 M_{s0}} \left( \frac{\partial \lambda}{\partial H} \right)_0 + \rho \frac{T}{T_c} \frac{\partial T_c}{\partial p} \frac{\partial M_s}{\partial T}, \quad (2)$$

where $\rho$ is density, $M_s$ is spontaneous magnetization, $(\frac{\partial \lambda}{\partial H})_0$, $M_{s0}$, and $\rho_0$ are the values of $\frac{\partial \lambda}{\partial H}$, $M_s$, and $\rho$ at 0 K. In an FM system, the divergence of $\frac{\partial M_s}{\partial T}$ around $T_C$ in a second-order phase transition from the $T < T_C$ side is responsible for the di-

vergence behavior in a piezomagnetic coefficient and the ME signal accordingly [30]. In an AFM system, $M_s$ is zero before and after Néel temperature $T_N$, leading to a featureless ME signal in MBT. For the $T > T_C$ side, spin-spin correlations and the ME signals are also related. Based on previous studies, the spin-spin correlation function $\langle S_f \cdot S_j \rangle$ is proportional to the magnetostriction $\lambda(H, T)$ around the phase transition. As a result, near ordering temperature, $\frac{\partial \lambda}{\partial H}$ is governed by spin-spin correlations that [18]

$$\frac{\partial \lambda}{\partial H} \approx 4 \sum_{j(f,g)} \tilde{D}_{11}^\alpha(f, g) \langle S_j^z S_f \cdot S_g \rangle, \quad (3)$$

where $\tilde{D}_{11}^\alpha(f, g)$ are the phenomenological two-ion magnetoelastic coupling constants between distinct nearest neighbor ion pairs $(f, g)$. $S_j^z$ is the component of spin $j$ along the external magnetic field direction and will go over all the spin sites. From Eqs. (1) and (3), a direct relationship between $V_x$ and $\langle S_j^z S_f \cdot S_g \rangle$ can be inferred. Note that, for the magnetically ordered systems like CGT and MBT, $\langle S_j^z S_f \cdot S_g \rangle$ and $\langle S_f \cdot S_g \rangle$ are related but different. At zero field, $\langle S_j^z S_f \cdot S_g \rangle$ is zero in the PM phase since $\langle S_j^z \rangle$ is zero, while under a finite magnetic field, both $\langle S_j^z S_f \cdot S_g \rangle$ and $\langle S_f \cdot S_g \rangle$ can persist well above ordering $T$ together with different decaying speeds. That is due to the combined decay of $\langle S_j^z \rangle$ and $\langle S_f \cdot S_g \rangle$ around $T_C$ or $T_N$ in $\langle S_j^z S_f \cdot S_g \rangle$. In CST and CGT, finite $\langle S_f \cdot S_g \rangle$ slowly decays well above $T_C$ by neutron scattering, second harmonic generation, and thermal expansion experiments [11,15,16], etc., while $V_x \propto d\lambda/dH$ fully decays up to temperatures twice that of $T_C$. An enhancement of $\langle S_j^z S_f \cdot S_g \rangle$ is expected in finite fields around $T_C$. At a fixed temperature in the PM phase, $\langle S_j^z \rangle$ will increase with the increasing magnetic field, while spin fluctuations will decrease with the increasing field. Such contrasting behaviors will lead to a peak feature for $\langle S_j^z S_f \cdot S_g \rangle$ at the finite field around $T_C$ and should be located at TP in CGT and CST. However, zero $V_x$ above $T_N$ indicate a null correlation function $\langle S_f \cdot S_g \rangle$ in MBT.

We now discuss the nature of TPs in the phase diagram of CST and CGT. Judging from thermodynamic criteria, in CST, the phase boundary between FM and PM is a second order in nature [13,14,23]; the boundary between FM and SP, in uniaxial magnets for $H$ along an easy axis, is also a second order line, but the boundary between SP and PM phases seems to be a crossover according to the previous specific heat and temperature-dependent magnetization measurements in the literature [10]. Also, no enhancement in specific heat around TP is found in CGT [10]. In this sense, the TP in CST differs from the critical point at $H = 0$ and $T = T_C$ proposed in Ref. [14] or the TP and tricritical point in MBT near which the order of the spin-flop transition changes its character from first to second order. In CST and CST cases, the TP should be a state where FM, PM, and SP phases coexist simultaneously. The physical properties must be exotic at this point, like the triple point in water.

We establish a technique for magnetostrictive properties with more information in the imaginary part from the above experimental results. This composite ME technique is a highly sensitive probe of domain dynamics, spin-spin correlations and their associated magnetostrictive properties, which are complementary to the capacitance dilatometry

method. This technique will be particularly superior for studying the quasi-two-dimensional magnetic system with a thin-thickness single crystal, which tends to have a much smaller absolute change along the thickness direction and is hard to be loaded in the capacitance dilatometry for in-plane measurements. It is also a fast and low-cost technique for exploring the magnetic phase diagram of bulk magnetic materials. It usually requires a longer time and multiple tools with expensive instruments, like capacitance dilatometry, ac susceptibility, magnetization, and neutron diffraction. This approach can offer spin-spin correlations in more antiferromagnetic or spin-glass systems and probe critical fluctuation around a tricritical or quantum critical point.

## IV. CONCLUSION

In conclusion, we have performed a comprehensive experimental study on the phase diagrams and spin-spin correlations of quasi-2D ferromagnetic $Cr_2Ge_2Te_6$ and $Cr_2Si_2Te_6$ and antiferromagnetic $MnBi_2Te_4$ by a sensitive composite magnetoelectric method. The magnetoelectric signals get greatly enhanced near FM and spin-flop transitions. We also

constructed the phase diagrams of the three compounds and found a triple point around Curie temperature where three phases coexist in the phase diagrams of $Cr_2Ge_2Te_6$ and $Cr_2Si_2Te_6$. By comparison, there is a triple or tricritical point in $MnBi_2Te_4$ only for $H$ along the $c$ axis. Most importantly, we observed an anomalous enhancement of magnetoelectric voltage near the triple point of $Cr_2Ge_2Te_6$ and $Cr_2Si_2Te_6$. That indicates a significant enhancement of ferromagnetic spin-spin correlations near this point. However, no short-range spin-spin correlation is found in $MnBi_2Te_4$ above Néel temperature.

[1] B. Huang, G. Clark, E. Navarro-Moratalla, D. R. Klein, R. Cheng, K. L. Seyler, D. Zhong, E. Schmidgall, M. A. McGuire, D. H. Cobden *et al.*, Layer-dependent ferromagnetism in a van der Waals crystal down to the monolayer limit, Nature (London) **546**, 270 (2017).

[2] C. Gong, L. Li, Z. Li, H. Ji, A. Stern, Y. Xia, T. Cao, W. Bao, C. Wang, Y. Wang *et al.*, Discovery of intrinsic ferromagnetism in two-dimensional van der Waals crystals, Nature (London) **546**, 265 (2017).

[3] C. Zhang, L. Wang, Y. Gu, X. Zhang, X. Xia, S. Jiang, L.-L. Huang, Y. Fu, C. Liu, J. Lin *et al.*, Hard ferromagnetic behavior in atomically thin CrSiTe₃ flakes, Nanoscale **14**, 5851 (2022).

[4] Z. Fei, B. Huang, P. Malinowski, W. Wang, T. Song, J. Sanchez, W. Yao, D. Xiao, X. Zhu, A. F. May *et al.*, Two-dimensional itinerant ferromagnetism in atomically thin Fe₃GeTe₂, Nat. Mater. **17**, 778 (2018).

[5] Y. Deng, Y. Yu, M. Z. Shi, Z. Guo, Z. Xu, J. Wang, X. H. Chen, and Y. Zhang, Quantum anomalous Hall effect in intrinsic magnetic topological insulator MnBi₂Te₄, Science **367**, 895 (2020).

[6] J. Als-Nielsen and R. J. Birgeneau, Mean field theory, the Ginzburg criterion, and marginal dimensionality of phase transitions, Am. J. Phys. **45**, 554 (1977).

[7] K. S. Burch, D. Mandrus, and J. G. Park, Magnetism in two-dimensional van der Waals materials, Nature (London) **563**, 47 (2018).

[8] N. Cao, X. Chen, X. Mi, S. Qiao, L. Zhang, K. Peng, M. He, A. Wang, Y. Chai, and X. Zhou, Angle dependent field-driven reorientation transitions in uniaxial antiferromagnet MnBi₂Te₄ single crystal, Appl. Phys. Lett. **120**, 163102 (2022).

[9] J. Zeisner, A. Alfonsov, S. Selter, S. Aswartham, M. P. Ghimire, M. Richter, J. van den Brink, B. Büchner, and V. Kataev, Mag-

netic anisotropy and spin-polarized two-dimensional electron gas in the van der Waals ferromagnet Cr₂Ge₂Te₆, Phys. Rev. B **99**, 165109 (2019).

[10] S. Selter, G. Bastien, A. U. B. Wolter, S. Aswartham, and B. Büchner, Magnetic anisotropy and low-field magnetic phase diagram of the quasi-two-dimensional ferromagnet Cr₂Ge₂Te₆, Phys. Rev. B **101**, 014440 (2020).

[11] T. J. Williams, A. A. Aczel, M. D. Lumsden, S. E. Nagler, M. B. Stone, J. Q. Yan, and D. Mandrus, Magnetic correlations in the quasi-two-dimensional semiconducting ferromagnet CrSiTe₃, Phys. Rev. B **92**, 144404 (2015).

[12] V. Carteaux, F. Moussa, and M. Spiesser, 2D ising-like ferromagnetic behaviour for the lamellar Cr₂Si₂Te₆ compound: A neutron scattering investigation, Europhys. Lett. **29**, 251 (1995).

[13] Y. Liu and C. Petrovic, Critical behavior of quasi-two-dimensional semiconducting ferromagnet Cr₂Ge₂Te₆, Phys. Rev. B **96**, 054406 (2017).

[14] G. T. Lin, H. L. Zhuang, X. Luo, B. J. Liu, F. C. Chen, J. Yan, Y. Sun, J. Zhou, W. J. Lu, P. Tong *et al.*, Tricritical behavior of the two-dimensional intrinsically ferromagnetic semiconductor CrGeTe₃, Phys. Rev. B **95**, 245212 (2017).

[15] A. Ron, E. Zoghlin, L. Balents, S. D. Wilson, and D. Hsieh, Dimensional crossover in a layered ferromagnet detected by spin correlation driven distortions, Nat. Commun. **10**, 1654 (2019).

[16] S. Spachmann, A. Elghandour, S. Selter, B. Büchner, S. Aswartham, and R. Klingeler, Strong effects of uniaxial pressure and short-range correlations in Cr₂Ge₂Te₆, Phys. Rev. Res. **4**, L022040 (2022).

[17] D. Lujan, J. Choe, M. Rodriguez-Vega, Z. Ye, A. Leonardo, T. N. Nunley, L.-J. Chang, S.-F. Lee, J. Yan, G. A. Fiete *et al.*, Magnons and magnetic fluctuations in atomically thin MnBi₂Te₄, Nat. Commun. **13**, 2527 (2022).

[18] E. Callen and H. B. Callen, Magnetostriction, forced magnetostriction, and anomalous thermal expansion in ferromagnets, Phys. Rev. **139**, A455 (1965).

[19] Z. Li, D. Xu, X. Li, H. Liao, X. Xi, Y. Yu, and W. Wang, Anomalous spin dynamics in a two-dimensional magnet induced by anisotropic critical fluctuations, Phys. Rev. B **106**, 054427 (2022).

[20] Y. Chai, P. Lu, H. Du, J. Shen, Y. Ma, K. Zhai, L. Wang, Y. Shi, H. Li, W. Wang *et al.*, Probe of skyrmion phases and dynamics in MnSi via the magnetoelectric effect in a composite configuration, Phys. Rev. B **104**, L100413 (2021).

[21] G. Srinivasan, Magnetoelectric composites, Annu. Rev. Mater. Res. **40**, 153 (2010).

[22] X. Zhang, Y. Zhao, Q. Song, S. Jia, J. Shi, and W. Han, Magnetic anisotropy of the single-crystalline ferromagnetic insulator $Cr_2Ge_2Te_6$, Jpn. J. Appl. Phys. **55**, 033001 (2016).

[23] B. Liu, Y. Zou, L. Zhang, S. Zhou, Z. Wang, W. Wang, Z. Qu, and Y. Zhang, Critical behavior of the quasi-two-dimensional semiconducting ferromagnet $CrSiTe_3$, Sci. Rep. **6**, 33873 (2016).

[24] D. Patil, J.-H. Kim, Y. S. Chai, J.-H. Nam, J.-H. Cho, B.-I. Kim, and K. H. Kim, Large longitudinal magnetoelectric coupling in $NiFe_2O_4$–$BaTiO_3$ laminates, Appl. Phys. Express **4**, 073001 (2011).

[25] E. W. Lee, Magnetostriction and magnetomechanical effects, Rep. Prog. Phys. **18**, 184 (1955).

[26] A. N. Bogdanov, A. V. Zhuravlev, and U. K. Rößler, Spin-flop transition in uniaxial antiferromagnets: Magnetic phases, reorientation effects, and multidomain states, Phys. Rev. B **75**, 094425 (2007).

[27] A.-B. M. A. Ibrahim, R. Murgan, M. K. A. Rahman, and J. Osman, *Morphotropic Phase Boundary in Ferroelectric Materials* (IntechOpen, London, 2011).

[28] T. N. Haidamak, J. Valenta, J. Prchal, M. Vališka, J. Pospíšil, V. Sechovský, J. Prokleška, A. A. Zvyagin, and F. Honda, Tricritical fluctuations and elastic properties of the Ising antiferromagnet $UIrSi_3$, Phys. Rev. B **105**, 144428 (2022).

[29] H. Tange and T. Tokunaga, Temperature dependence of the forced magnetostriction of nickel, J. Phys. Soc. Jpn. **27**, 554 (1969).

[30] R. M. Bozorth and T. Wakiyama, Magnetostriction and anomalous thermal expansion of single crystals of gadolinium, J. Phys. Soc. Jpn. **18**, 97 (1963).